Liquid Crystals
Publication details, including instructions for authors and subscription information:
http://www.informaworld.com/smpp/title~content=t713926090

Effects on thermo-optical properties of the composition of a polymer-stabilised liquid crystal with a smectic A-chiral nematic phase transition

Guohui Pan[a]; Lilong Yu[b]; Hongbin Zhang[a]; Jinbao Guo[a]; Renwei Guo[a]; Hui Cao[a]; Zhou Yang[a]; Huai Yang[a]; Siquan Zhu[ac]
[a] Department of Materials Physics and Chemistry, School of Materials Science and Engineering, University of Science and Technology Beijing, Beijing 100083, China [b] Compilation Office of Dalian University Newspaper, Dalian University, Dalian 116622, China [c] Opthalmology Department, Beijing Tongren Hospital, Capital Medical, Beijing 100730, China

To cite this Article Pan, Guohui , Yu, Lilong , Zhang, Hongbin , Guo, Jinbao , Guo, Renwei , Cao, Hui , Yang, Zhou , Yang, Huai and Zhu, Siquan(2008) 'Effects on thermo-optical properties of the composition of a polymer-stabilised liquid crystal with a smectic A-chiral nematic phase transition', Liquid Crystals, 35: 9, 1151 — 1160
To link to this Article: DOI: 10.1080/02678290802403950
URL: http://dx.doi.org/10.1080/02678290802403950

Liquid Crystals,
Vol. 35, No. 9, September 2008, 1151–1160

Taylor & Francis
Taylor & Francis Group

Effects on thermo-optical properties of the composition of a polymer-stabilised liquid crystal with a smectic A–chiral nematic phase transition

Guohui Pan[a], Lilong Yu[b], Hongbin Zhang[a], Jinbao Guo[a], Renwei Guo[a], Hui Cao[a], Zhou Yang[a], Huai Yang[a]* and Siquan Zhu[ac]

[a]*Department of Materials Physics and Chemistry, School of Materials Science and Engineering, University of Science and Technology Beijing, Beijing 100083, China;* [b]*Compilation Office of Dalian University Newspaper, Dalian University, Dalian 116622, China;* [c]*Opthalmology Department, Beijing Tongren Hospital, Capital Medical, Beijing 100730, China*

(Received 17 July 2008; final form 12 August 2008)

A photopolymerisable monomer/liquid crystal (LC)/chiral dopant/photoinitiator mixture with a smectic A (SmA*)–chiral nematic (N*) phase transition was prepared. After the SmA* phase was homeotropically oriented and then irradiated by ultraviolet light, a homeotropically oriented polymer network was formed in the SmA* phase and then a homeotropically oriented polymer network-stabilised liquid crystal (PSLC) film with a SmA*–N* phase transition was prepared. In the temperature range of the SmA* phase, the LC molecules were homeotropically oriented and the film exhibited a transparent state. However, in the temperature range of the N* phase, the film exhibited a strong light-scattering state owing to the fact that the LC molecules adopted a focal conic alignment affected by the homeotropically oriented polymer network. The strong light-scattering state of the N* phase could be changed into a transparent one when an electric field was applied. The focus of this study was on the effects of composition of the PSLC film on its thermo-optical and electro-optical properties.

Keywords: PSLC; smectic A–chiral nematic transition; thermo-optical properties; electro-optical properties

1. Introduction

Polymer-stabilised liquid crystal (PSLC) films have provided a new field of LC science and technology (*1–15*), in which a desired macroscopic orientation of LC directors can be stabilised (*1–8*) or frozen (*9*) by the crosslinked network dispersed within the LC. For example, a three-dimensional cubic structure with lattice period of several hundred nanometres in its blue phase, of which the temperature range is usually less than a few kelvins, can be stabilised over a temperature range of more than 60 K (*5*). The planar molecular alignment of a chiral nematic (N*) phase can also be stabilised in a chiral smectic A (SmA*) phase at the macroscopic level, enabling the SmA* phase to have optical characteristics similar to those of an N* phase and the mechanical properties of a SmA* phase (*6*). Moreover, PSLC films with gradient pitch distribution and non-uniform pitch distribution have also been prepared for use as brightness-enhancement films in LC displays (*7–12*). In addition, PSLC films have many other potential applications, including light shutters (*1–5*), E-papers (*6*), wide-band polarisers (*7–12*) and reflective LC displays (*13–15*).

The thermo-optical properties of a PSLC film with a SmA*–N* phase transition have been studied by Yang *et al.* (*16*). The PSLC film was prepared by ultraviolet (UV) radiation-induced crosslinking between the molecules of a photopolymerisable monomer in the homeotropically oriented SmA* phase of the photopolymerisable monomer/LC/photoinitiator mixture with a SmA*–N* phase transition. On heating the PSLC film from the SmA* to the N* phase, a sharp change occurs from a transparent to a light-scattering state. On cooling from the N* to the SmA* phase, the PSLC film can change from the light scattering to the transparent state reversibly. However, the effects of the composition of the PSLC film on its thermo-optical properties have not been studied.

In this paper, the effects of the composition of the PSLC film on its thermo-optical properties as well as on the electro-optical properties of the N* phase of the PSLC film are reported.

2. Experiments

Materials

The nematic LC, SLC-1717 (Shijiazhuang Yongsheng Huatsing Liquid Crystal Co., Ltd, Shijiazhuang City, Hebei Province, China), the chiral dopant, S811 (Merck Co., Ltd), and the photoinitiator, 2,2-dimethopxy-1,2-diphenylethanone (IRG651, TCI Co., Ltd) were used. The SmA LC was prepared from cyanobiphenyls (nCBs). The nCBs and the photopolymerisable LC diacrylate monomer, C6M, were synthesised accord-

*Corresponding author. Email: yanghuai@mater.ustb.edu.cn

ISSN 0267-8292 print/ISSN 1366-5855 online

DOI: 10.1080/02678290802403950
http://www.informaworld.com

(1) Photo-polymerizable LC monomer: C6M

Cr 356.4 N 388.8 I

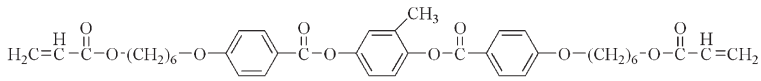

(2) Smectic-A LC: nCB

Mixture of LCs with positive dielectric anisotropy

Cr 261.7 SmA 318.4 N 319.6 I

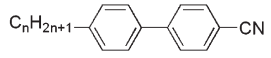

n=8: 50.4wt% n=10: 21.6wt%

n=11: 18.0wt% n=12: 10.0wt%

(3) Nematic LC: SLC1717 (Yongsheng Huatsing Liquid Crystal Co., Ltd.)

Mixture of LCs with positive dielectric anisotropy

Cr 233.0 N 365.0 I

(4) Chiral Dopant: S811 (Merck Co., Ltd.)

Left-handed

Cr 320.2 I

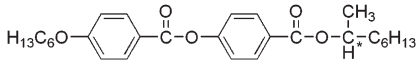

(5) Photoinitiator: 2, 2-dimethopxy-1, 2-diphenyl-ethanone (TCI Co., Ltd.)

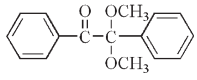

Figure 1. Chemical structures and some physical parameters of the materials used.

ing to the methods suggested by Gray *et al.* (*17*) and Broer *et al.* (*18*), respectively. Figure 1 shows the chemical structures and some physical parameters of the above materials.

Preparation of samples

In order to induce homeotropic orientation of the LC molecules, the inner surfaces of indium tin oxide (ITO)-coated glass cells were treated with *N*,*N*-dimethyl-*N*-octadecyl-3-aminopropyltrimethoxysilyl chloride (DMOAP) solution (0.1% by volume in water) (*19*). Poly(ethylene terephthalate) (PET) films (20 μm thick) were used as the cell spacers.

To prepare the PSLC film, the samples of C6M/LC/S811/photoinitiator mixtures were filled into the cells by capillary action in the N* phase. Then the homeotropically oriented SmA* phase of the samples was irradiated by UV light (365.0 nm, 1.1 mW cm^{-2}) for half an hour at 301.2 K to induce crosslinking between the molecules of C6M in the samples.

Measurements

The phase transition temperatures and the aggregation structure of the samples used were determined using differential scanning calorimetry (DSC, Perkin-Elmer DSC 6) at a heating rate of 10.0 K min^{-1} and polarising optical microscopy (POM, Olympus BX-51) at a heating rate of 1.0 K min^{-1}. The thermo-optical and electro-optical performances were investigated with a LC display parameters tester (LCT-5016C, Changchun Lianchen Instrument Co, Ltd, China). The polymer networks for scanning electron microscopy (SEM, Cambridge S360) observations were prepared in the following way. After UV irradiation of the cell for photopolymerisation, the sealant material of the cell was removed to allow diffusion of hexane into the cell. After extracting the LC with hexane, the cell was dried *in vacuo* for a few hours. Then, the cell was opened with caution and the substrate plus polymer network were coated with thin gold layer to eliminate any electric charge problems for SEM study.

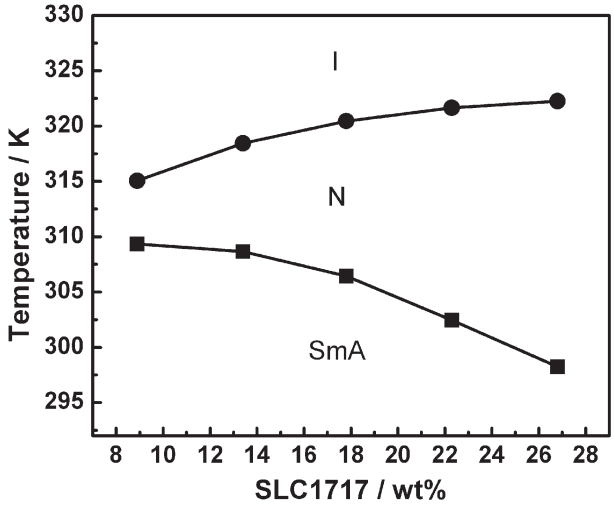

Figure 2. Variation with content of SLC1717 of the phase transition temperatures.

3. Results and discussion

The dependence on SLC1717 and S811 content of the phase transition temperatures of SmA LC (nCB)/N LC (SLC1717) and nCB/SLC1717/S811 composites is shown in Figures 2 and 3, respectively. Figure 2 shows that the temperature of the SmA–N phase transition for the nCB/SLC1717 composite decreases with increasing the content of SLC1717, owing to the fact that SLC1717 is a N LC at room temperature, whereas the temperature of the N–isotropic (I) phase transition temperature of the composite increases with increasing the content of SLC1717, owing to the N–I phase transition temperature of SLC1717 being higher than those of nCB. Figure 3 shows that the temperatures of both the SmA*–N* and the N*–I phase transitions decrease with increasing content of S811 because S811 is non-mesogenic. Thus, the SmA*–N* phase transition temperature of nCB/SLC1717/S811 composite could be changed by adjusting the composition. The compositions of the studied samples are listed in Table 1.

Table 1. Composition of the samples investigated.

Sample	C6M/liquid crystal (nCB/SLC1717)/S811 /wt%
A1	2.0/91.1 (73.0/18.1)/6.9
A2	3.0/90.2 (72.2/18.0)/6.8
A3	4.0/89.3 (71.4/17.9)/6.7
A4	5.0/88.3 (70.6/17.7)/6.7
A5	6.0/87.4 (70.0/17.4)/6.6
B1	4.0/91.2 (77.5/13.7)/4.8
B2	4.0/90.2 (76.7/13.5)/5.8
B3	4.0/89.3 (75.9/13.4)/6.7
B4	4.0/88.3 (75.0/13.3)/7.7
B5	4.0/87.4 (74.3/13.1)/8.6
C	0.0/93.0 (69.7/23.3)/7.0

In order to understand better the effect of the polymer network on the thermo-optical properties of the studied PSLC films, the thermo-optical properties of sample C without polymer network was first investigated. Figure 4 shows the temperature dependence of the transmittance of sample C. Since the inner surfaces of the cell containing sample C had been treated for homeotropic orientation of LC molecules, the LC molecules of the SmA* phase of sample C were homeotropically oriented and the SmA* phase was transparent. On heating sample C from the SmA* to the N* phase, a sharp change in the transmittance from about 95% to about 20% occurred. On cooling sample C from the N* to the SmA* phase at a rate of $1.0\,\mathrm{K\,min^{-1}}$, the SmA* phase was homeotropically oriented and became transparent again. However, if the sample was quenched in water at 273.2 K, the light-scattering

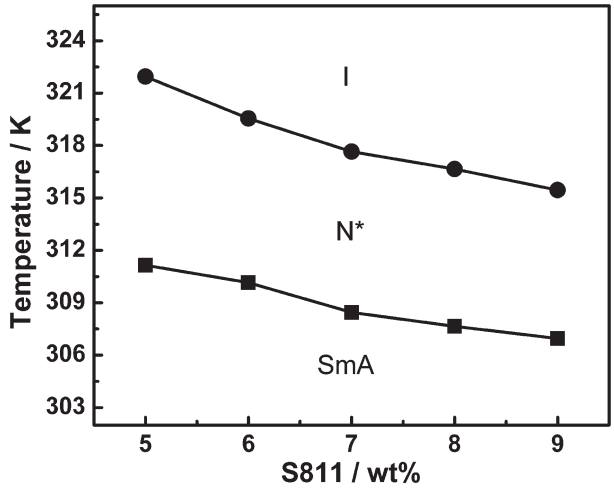

Figure 3. Variation with content of chiral dopant of the phase transition temperatures.

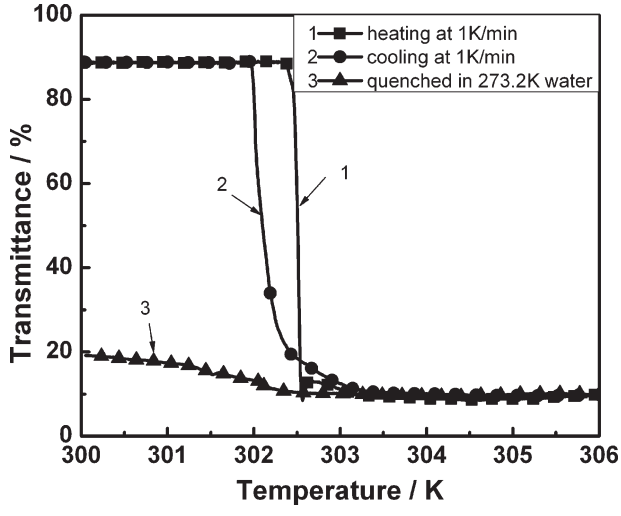

Figure 4. Variation with temperature of the transmittance for sample C.

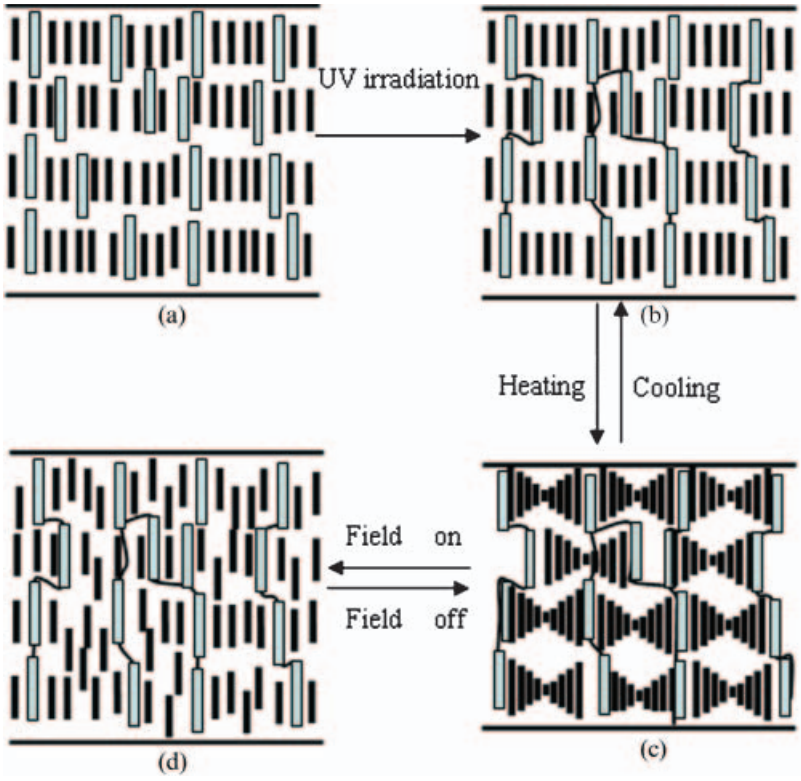

Figure 5. Schematic diagram of film preparation.

state of the N* phase could mostly be stored in the SmA* phase, and then the SmA* phase also exhibited light scattering.

Figure 5 shows a schematic representation of the preparation process of the expected PSLC film. At first, the C6M/LC/S811/photoinitiator mixture was filled into the cell and was cooled to the SmA* phase of the mixture, as shown in Figure 5(a). On cooling the mixture to the SmA* phase, the SmA* phase was homeotropically oriented by the surface orientation agent. After the SmA* phase was irradiated by UV light, a homeotropically oriented polymer network formed from crosslinking between the molecules of C6M was formed in the SmA* phase; thus the PSLC film was transparent, as shown in Figure 5(b). The film could be changed to a strong light-scattering state (Figure 5(c)) accompanied by a texture change from the homeotropic texture of the SmA* phase to the focal conic texture of N* on heating above the SmA*–N* phase transition temperature, owing to both the anchoring effect of the polymer network and the orientation effect of the surface orientation agent. Fundamentally, the long axes of LC molecules in the vicinity of the homeotropic polymer tended to remain perpendicular to the cell surfaces, whereas the remaining LC relaxed back to the spiral structure, i.e. a focal conic texture was formed as the result of the competition between the intrinsic spiral structure and the constraining effect of the polymer network (*3*). The light-scattering effect was attributed to the mismatch of refractive indices between the small focal conic domains (*20, 21*). On being cooled from the N* to the SmA* phase, the film went back to the transparent state (Figure 5(b)). On application of an electric filed, the strongly light-scattering state was changed into the transparent one, owing to the fact that the LC molecules with a positive dielectric anisotropy were homeotropically aligned by the applied electric field (Figure 5(d)).

Figure 6(a) shows the temperature dependence of the transmittances for the composites prepared from samples A1–A5. As can be seen from Figure 6(a), the transition between the transparent state and strongly light-scattering one was so sharp that it could be realised in a temperature range of about 0.2 K when the heating rate was $1\,\mathrm{K\,min^{-1}}$. This is because the SmA*–N* phase transition is a very weak first-order or second-order transition (*22, 23*), and the temperature range of coexistence of SmA* and N* phases is very narrow. The transmittance of transparent state in the range of 80–90% showed excellent light transmitting property, while the transmittance of light scattering state of some of the samples was less than 1.0%, showing good light-blocking properties. The loss of light intensity in the transparent state was mainly due to the reflections from the glass–air

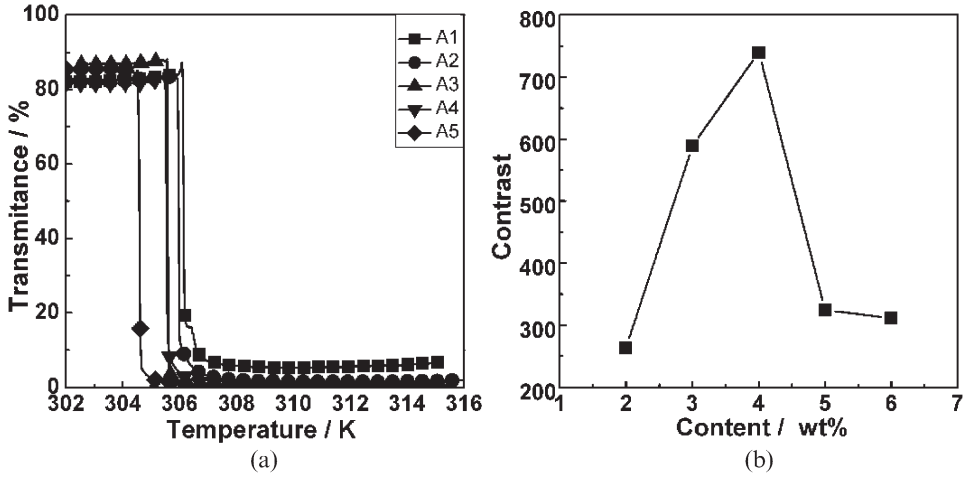

(a) (b)

Figure 6. Variation with (a) temperature of the transmittance and (b) with content of polymer network of the thermo-optical contrast of samples A1–A5.

interfaces (*3*). If the thermo-optical contrast is defined as the ratio of the highest transmittance in transparent state to the lowest transmittance in light scattering state, as shown in Figure 6(b), the thermo-optical contrast peaked at 4.0 wt% of the polymer network. This should be because the tendency for the LC molecules to form a focal conic texture increased with increasing the content of the polymer network when the content was smaller than 4.0 wt%, whereas the tendency for the LC molecules to be aligned homeotropically affected by the polymer network increased with increasing the content when the content was larger that 4.0 wt%.

Figure 7(a) shows the temperature dependence of the transmittance for the composites prepared from samples B1–B5, and Figure 7(b) shows the dependence on content of the chiral dopant of the thermo-optical contrast, which shows that the thermo-optical contrast peaks at 6.7 wt%. This result indicates that the sample with 6.7% of chiral dopant had the appropriate light-scattering domains with the fixed content of the polymer network; in other words, the pitch length was one of the factors determining the light-scattering intensity. If the pitch was long, the domain size was too large to scatter light strongly, whereas in the opposite condition, the domain size was too small to scatter light strongly.

Figure 8 shows the dependence on content of the polymer network of the electro-optical properties for the composites prepared from samples A1–A5. A change from the focal conic texture (Figure 5(c)) to homeotropic one (Figure 5(d)) was realised when the electric field was applied to the N* phase. This change was realised when the LC molecules had a positive dielectric anisotropy and an electric field higher than a critical value, $E_c = \frac{\pi^2}{p_o}\sqrt{\frac{K_{22}}{\varepsilon_o \Delta\varepsilon}}$, was applied

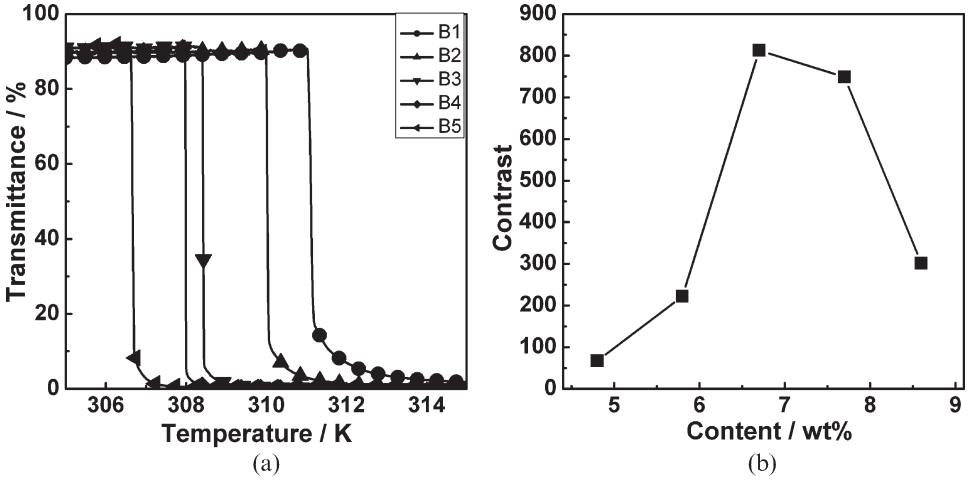

(a) (b)

Figure 7. Variation with (a) temperature of the transmittance and (b) with content of chiral dopant of the thermo-optical contrast of samples B1–B5.

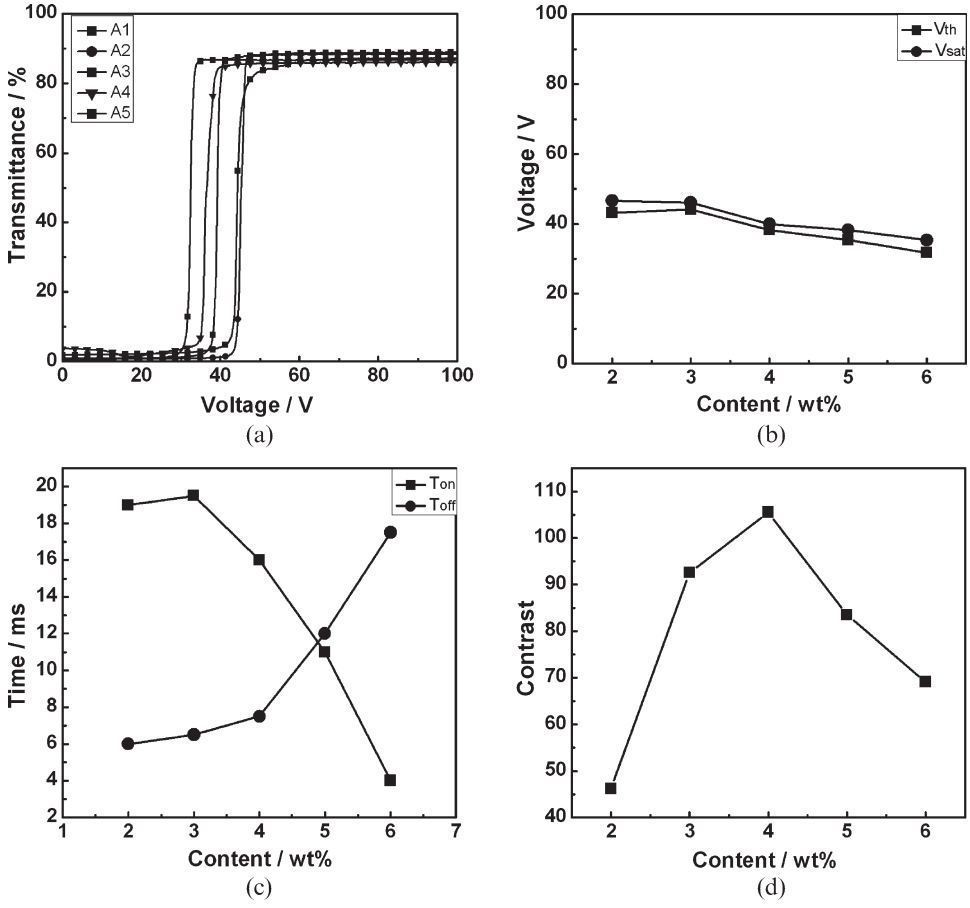

Figure 8. Variation with (a) voltage of the transmittance and with content of polymer network of (b) V_{th} and V_{sat}, (c) T_{on} and T_{off} and (d) contrast ratio for samples A1–A5.

(*24, 25*). The measured electro-optical parameters included the threshold voltage (V_{th}), the saturation voltage (V_{sat}), the field-on response time (T_{on}) and the field-off response time (T_{off}). The threshold voltage (V_{th}) and the saturation voltage (V_{sat}) are defined as the voltage required for the transmittance to reach 10% and 90%, respectively. T_{on} and T_{off} are defined as the time for the transmittance going from 10% to 90% (or 90% to 10%) of the total change between the on and off states. The contrast ratio is defined as the larger of the two transmittance values divided by the smaller of the two values. The voltage dependence of the transmittance is shown in Figure 8(a) and the dependence on content of the polymer network of V_{th} and V_{sat} is shown in Figure 8(b). As can be seen in Figures 8(a) and 8(b), both V_{th} and V_{sat} decreased a little with increasing polymer network content, which is due to the elastic interaction between the polymer network and LC molecules becoming stronger with increasing content of the polymer network, so less energy was needed to complete the unwind process. The dependence on content of the polymer network of T_{on} and T_{off} is shown in Figure 8(c). As shown in Figure 8(c), T_{on} decreased with increasing content of the polymer network, whereas T_{off} increased with the increase of the content, which should be due to the fact that less time was needed for the LC molecules to unwind their helical structure. However, more time was required for the LC molecules to go back to their original helical structure with increasing content since the elastic interaction between the LC molecules and the polymer network became stronger with increasing content, as mentioned above. The dependence on content of the polymer network of the contrast ratio is shown in Figure 8(d), which shows that the contrast ratio was a maximum at 4.0 wt%. This resulted from the fact that sample A3 had the maximum light-scattering intensity, due to the reasons already mentioned.

Figure 9 shows the dependence on content of the chiral dopant of the electro-optical properties. The voltage dependence of the transmittance of the samples with different content of the chiral dopant is shown in Figure 9(a) and the dependence content of the chiral dopant of the voltage is shown in Figure 9(b). As can be seen in Figures 9(a) and 9(b),

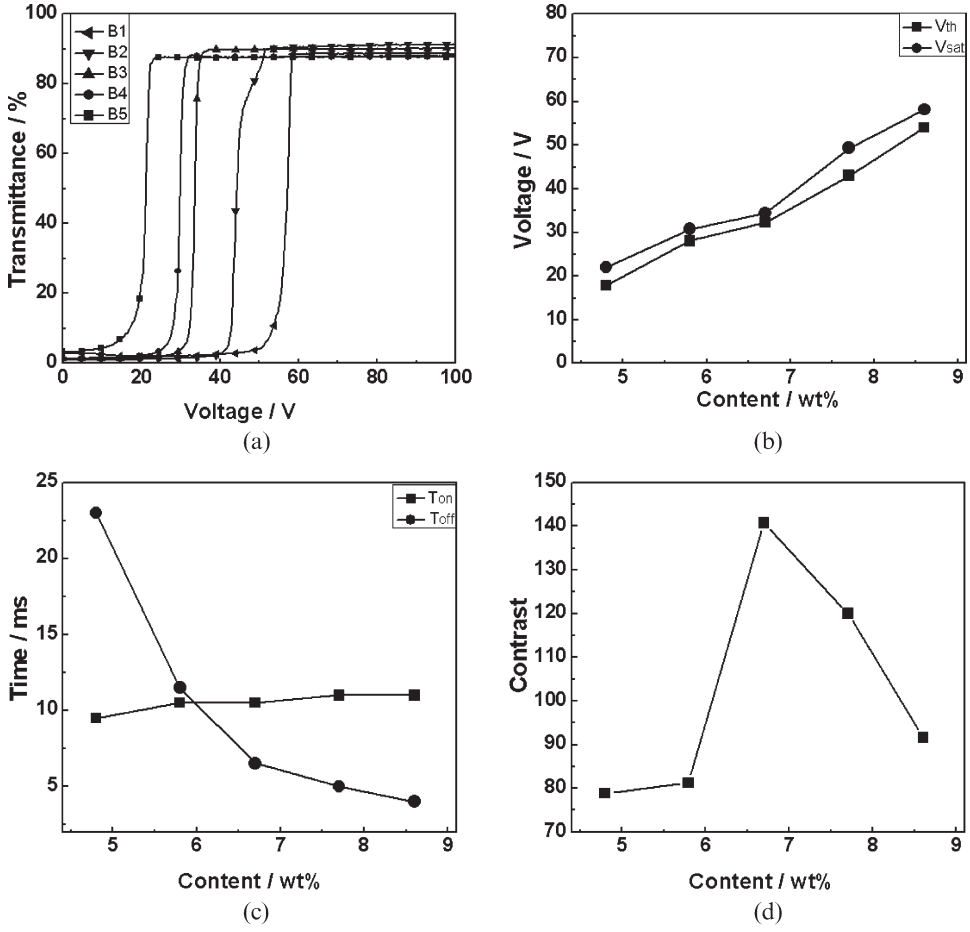

Figure 9. Variation with (a) voltage of the transmittance and content of chiral dopant of (b) V_{th} and V_{sat}, (c) T_{on} and T_{off} and (d) contrast ratio for samples B1–B5.

both V_{th} and V_{sat} increased with increasing content of the chiral dopant and they had an approximately linear dependence on the content. From the relationship between the critical value of the electric field (proportional to the voltage) and the pitch length of the LC as mentioned above, it could be concluded that V_{th} was in inverse proportional to the pitch length of the LC. Meanwhile, it is well known that the pitch length is inverse proportional to the content of the chiral dopant. Therefore, there is a linear relationship between the content of the chiral dopant and V_{th} $\left(V \propto \frac{1}{P} \propto C_c\right)$, which could be verified from Figure 9(b). From an energy viewpoint, it is reasonable to propose that more energy was needed to unwind the helical structure with the decreasing of the pitch length resulting from the increasing content of the chiral dopant. Figure 9(c) shows the dependence on content of the chiral dopant of T_{on} and T_{off}. As can be seen in Figure 9(c), T_{on} increased a little with increasing content of the chiral dopant, whereas T_{off} decreased. This result was in agreement with $\tau_{off} \propto \frac{1}{q_0^2} \propto \frac{1}{C_c^2}$. The contrast ratio also peaked at about 6.7 wt %, which further verified that strong light scattering was obtained when the size of the light scattering domain is controlled to certain value.

Figure 10 shows SEM photographs of the polymer network observed in different angles and amplifications. As shown in Figure 1, the monomer used comprises a mesogenic core, reactive end-groups and flexible alkyl spacer chains between the core and the end-groups (*3, 26*). The acrylate functional groups are attached to both sides of the mesogenic core by a flexible alkyl chain; the mesogenic core align the individual monomer molecules with local liquid crystalline order, whereas the flexible alkyl chains allow adjacent cores to align themselves parallel to one another during polymerisation (*27*). As mentioned above, the monomer was polymerised in homeotropic SmA*; during photopolymerisation the order of the SmA* phase was templated by the forming polymer network, so it is reasonable to say that the polymer network should be oriented homoetropically in the cell. Figure 10(a) shows the morphology of fractured surface of homeotropically

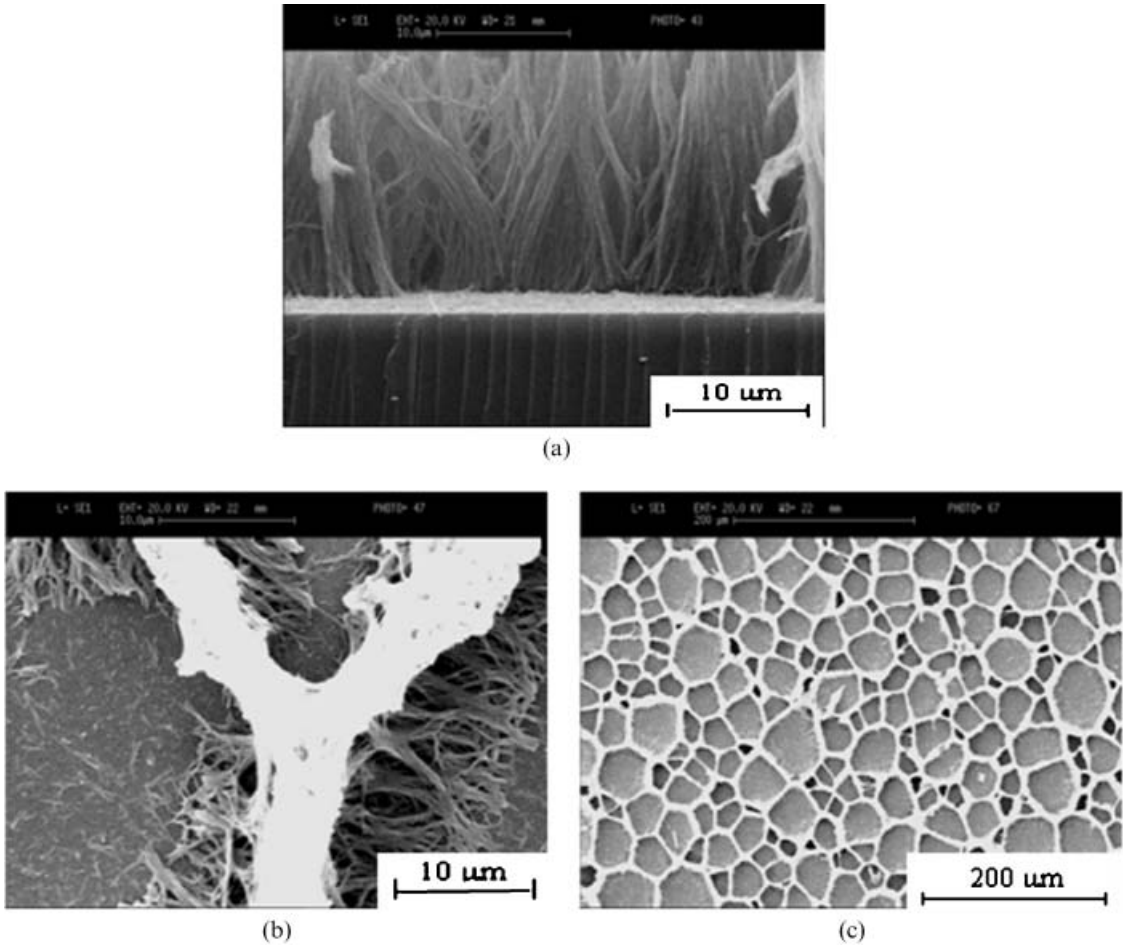

Figure 10. SEM photographs of the homeotropically oriented polymer network observed for angles between the observing direction and the normal of the substrate surface of about (a) 90.0°, (b) 0.0° and (c) 0.0° with different amplification.

oriented polymer network for sample A5 observing with a 90° angle between the observing direction and the normal direction of substrate surface from which the fibrous polymer network perpendicular to the substrate was observed. The polymer network composed of polymer strands oriented along the direction of the director. The smooth fibrous morphology of the polymer network was attributed to the good solubility of the monomer in LC. Generally, below the solubility limit, undergoing a radical chain polymerisation leads to smooth polymer network. This behaviour may be understood in the context of the Flory–Huggins model of polymer solubility, which is the primary factor determining the network morphology (*28*). As can be seen from Figures 10(b) and 10(c), when observed parallel to the normal direction of substrate surface, the formed fibre-shape polymer aggregated together like walls to divide the space into meshes in which the LC molecules existed. The white region shown in Figure 10(b) is from the aggregate effect of the polymer network.

Figure 11 shows the morphology of the polymer network in the composites prepared from samples A1–A5. As can be seen from Figure 11, the size of meshes of the polymer network decreased in the sequence. It is easy to understand that, increasing monomer content leads to denser polymer networks with smaller voids (*29, 30*). It has been demonstrated by our experiments that the sample with a content of more than 10.0 wt% polymer network could not change to the light scattering state on heating from the transparent state due to that the polymer network was too dense, and the mesh size was so small that the phase transition was completely limited by the polymer network. So the elastic interaction between the polymer network and the LC molecules had already entered the ''stable and clear'' region (*1*).

Figure 12 shows the morphology of the polymer network of the composites prepared from samples B1–B5. As can be seen from Figure 12, the content of the chiral dopant had little influence on the morphology of the polymer network.

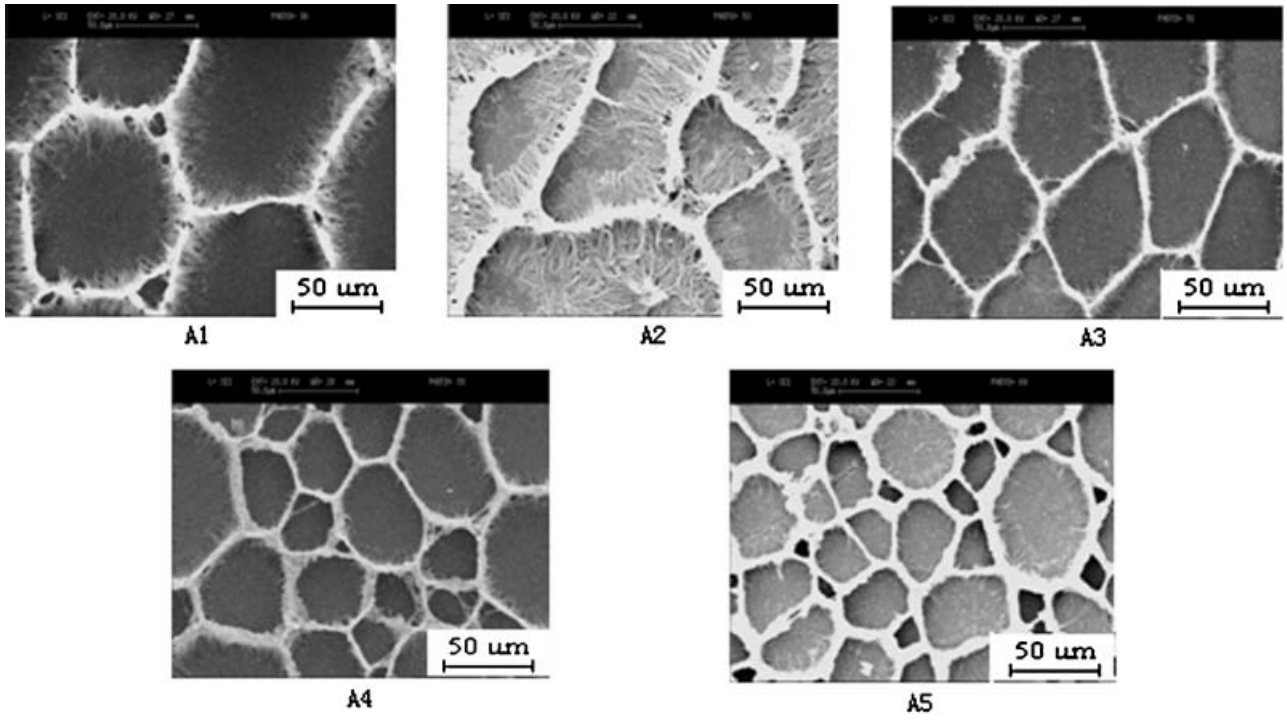

Figure 11. SEM photographs of the homeotropically oriented polymer network for samples A1–A5.

Figure 13 shows photographs of the cell. When the environmental temperature became higher than the SmA*–N* phase transition temperature, the cell changed from the transparent state (Figure 13(a)) into the light scattering state (Figure 13(b)), and vice versa.

4. Conclusions

In this study, polymer network/LC/chiral dopant composite films were prepared by photopolymerisation of LC monomer/LC/chiral dopant/photoinitiator

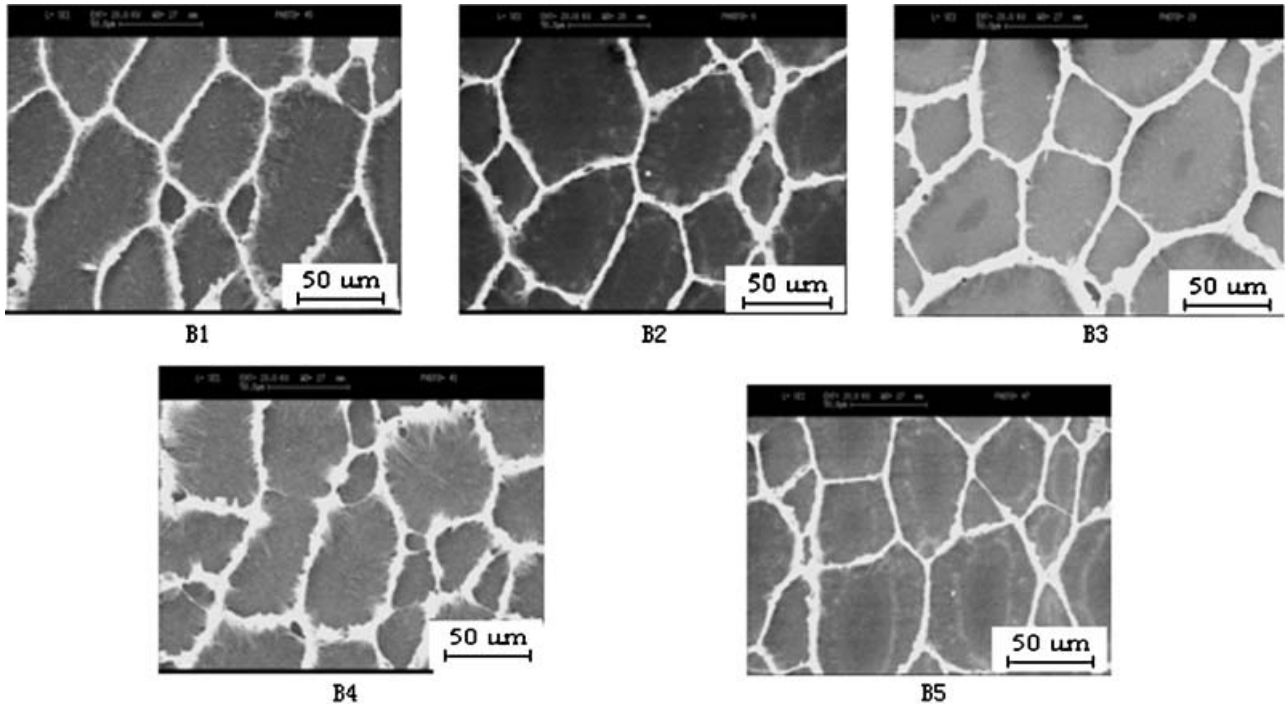

Figure 12. SEM photographs of the homeotropically oriented polymer network for samples B1–B5.

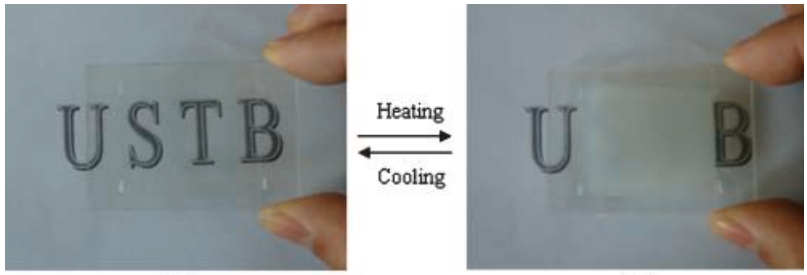

Figure 13. Photographs of the cell switching between the transparent state and the light-scattering state.

mixtures and the effects of the composition of the film on its thermo-optical and electro-optical properties investigated. The results indicate that the N* phase of the sample with 4.0 wt% polymer network and 6.7 wt% chiral dopant exhibited the strongest light-scattering intensity. The switching characteristics between the light-scattering state and the transparent one of the N* phase were also studied. Both of V_{th} and V_{sat} decreased and increased, respectively, with increasing contents of the polymer network and the chiral dopant. The T_{on} value decreased and increased, respectively, with increasing the contents of the polymer network and the chiral dopant, whereas T_{off} had the opposite changing tendency. SEM observation showed that increasing content of the monomer led to denser polymer network with smaller voids, whereas various content of the chiral dopant had no effect on the morphology of the polymer network. It is believed that the film has great potential for alarm devices of overheating or other thermo-electrical sensors.

Acknowledgements

Financial support from Hi-tech Research and Development Program of China (Grant No. 2006AA03Z108) and Projects of Chinese National Science and Technology Tackling Key Problems (Grant No. 2006BAI03A09) are gratefully acknowledged.

References

(1) Crawford G.P.; Zumer S. *Liquid Crystals in Complex Geometries*; Taylor & Francis: London, 1996. pp. 124–126.
(2) Broer D.J. *Radiation Curing in Polymer Science and Technology*; Elsevier Science: London, 1993. pp. 383–443.
(3) Yang D.K.; Chien L.C.; Doane J.W. *Appl. Phys. Lett.* **1992**, *60*, 3102–3104.
(4) Yang H.; Mishima K.; Matsuyama K.; Hayashi K.I.; Kikuchi H.; Kajiyama T. *Appl. Phys. Lett.* **2003**, *82*, 2407–2409.
(5) Kikuchi H.; Yokota M.; Hisakado Y.; Yang H.; Kajiyama T. *Nature Mater.* **2002**, *1*, 64–68.
(6) Yang H.; Kikuchi H.; Kajiyama T. *Chem. Lett.* **2003**, *32*, 256–257.
(7) Hikmet R.A.M.; Kemperman H. *Liq. Cryst.* **1999**, *26*, 1645–1653.
(8) Hikmet R.A.M.; Kemperman H. *Nature* **1998**, *392*, 476–479.
(9) Bian Z.Y.; Li K.; Huang W.; Cao H.; Yang H. *Appl. Phys. Lett.* **2007**, *91*, 201908–201910.
(10) Mitov M.; Dessaud N. *Nature Mater.* **2006**, *5*, 361–364.
(11) Relaix S.; Bourgerette C.; Mitov M. *Appl. Phys. Lett.* **2006**, *89*, 251907–251909.
(12) Ren H.W.; Wu S.T. *J. Appl. Phys.* **2002**, *92*, 797–800.
(13) Wu S.T.; Yang D.K. *Reflective Liquid Crystal Display*; Wiley: Singapore, 2001. pp. 197–198.
(14) Chien L.C.; Cho J.; Leroux N. *Proc. SPIE* **1998**, *129*, 3421–3427.
(15) Lu S.Y.; Chien L.C. *Appl. Phys. Lett.* **2007**, *91*, 131119–131121.
(16) Yang H.; Kikuchi H.; Kajiyama T. *Liq. Cryst.* **2000**, *27*, 1695–1699.
(17) Gray G.W.; Harrison K.J.; Nash J.A. *Electron. Lett.* **1973**, *9*, 130–131.
(18) Broer D.J.; Boven J.; Mol G.N. *Makromol. Chem.* **1989**, *190*, 2255–2268.
(19) Kahn F.J. *Appl. Phys. Lett.* **1973**, *22*, 386–388.
(20) Mochizuki A. *Proc. SID* **1990**, *31*, 155–120.
(21) Wysocki J.; Adams J.; Haas W. *Liquid Crystals*; Brown G.H. (Ed), Publisher?: New York, 1968. pp. 135–136.
(22) de Gennes P.G. *Solid St. Commun.* **1972**, *10*, 753–756.
(23) Lubensky T.C.; Renn S.R. *Phys. Rev. A* **1990**, *41*, 4392–4401.
(24) Chandrasekhar S. *Liquid Crystals*; Cambridge University Press: New York, 1992. pp. 135–136.
(25) Meyer R.B. *Appl. Phys. Lett.* **1969**, *14*, 208–209.
(26) Fung Y.K.; Yang D.K.; Ying S.; Chien L.C.; Zumer S.; Doane J.W. *Liq. Cryst.* **1995**, *19*, 797–801.
(27) Dierking I.; Kosbar L.L.; Lowe A.C.; Held G.A. *Appl. Phys. Lett.* **1997**, *71*, 2454–2456.
(28) Dierking I. *Adv. Mater.* **2000**, *12*, 167–181.
(29) Dierking I.; Kosbar L.L.; Afzali-Ardakani A.; Lowe A.C.; Held G.A. *J. Appl. Phys.* **1997**, *81*, 3007–3014.
(30) Mitov M.; Boudet A.; Sopena P.; Sixou P. *Liq. Cryst.* **1997**, *23*, 903–910.